

SERI/TR-252-3056  
DE87012282

September 1987

# Modeling High-Temperature Direct-Contact Heat Exchange in an Irrigated Packed Bed

Mark S. Bohn



# SERI

**Solar Energy Research Institute**

A Division of Midwest Research Institute

1617 Cole Boulevard  
Golden, Colorado 80401-3393

Operated for the  
**U.S. Department of Energy**  
under Contract No. DE-AC02-83CH10093

**SERI/TR-252-3056**  
**UC Category: 62a**  
**DE87012282**

# **Modeling High-Temperature Direct-Contact Heat Exchange in an Irrigated Packed Bed**

**Mark S. Bohn**

**September 1987**

**Prepared under Task No. 4275.100**  
**FTP No. 12-593**

## **Solar Energy Research Institute**

A Division of Midwest Research Institute

1617 Cole Boulevard  
Golden, Colorado 80401-3393

Prepared for the

**U.S. Department of Energy**  
Contract No. DE-AC02-83CH10093

#### NOTICE

This report was prepared as an account of work sponsored by the United States Government. Neither the United States nor the United States Department of Energy, nor any of their employees, nor any of their contractors, subcontractors, or their employees, makes any warranty, expressed or implied, or assumes any legal liability or responsibility for the accuracy, completeness or usefulness of any information, apparatus, product or process disclosed, or represents that its use would not infringe privately owned rights.

Printed in the United States of America  
Available from:  
National Technical Information Service  
U.S. Department of Commerce  
5285 Port Royal Road  
Springfield, VA 22161

Price: Microfiche A01  
Printed Copy A03

Codes are used for pricing all publications. The code is determined by the number of pages in the publication. Information pertaining to the pricing codes can be found in the current issue of the following publications, which are generally available in most libraries: *Energy Research Abstracts*, (*ERA*); *Government Reports Announcements and Index* (*GRA* and *I*); *Scientific and Technical Abstract Reports* (*STAR*); and publication, NTIS-PR-360 available from NTIS at the above address.

**PREFACE**

The research and development described in this document was conducted within the U.S. Department of Energy's Energy Storage Technology Program. The Solar Energy Research Institute (SERI) is the lead laboratory for research, technology, and system analyses and assessments for thermal energy storage for solar thermal applications and for thermal energy transport.

The goal of SERI's Solar Energy Storage Program is to identify economical energy storage and transport subsystems for the industrial sector and to bring the corresponding technologies to the point where they can be transferred from research to development. The strategy to accomplish this goal is to conduct research in advanced thermal energy storage technologies for solar thermal electric power and solar thermal industrial process heat applications, and in energy transport technologies for industrial process heat applications.

The focus of the program is in developing containment techniques and heat exchange for high temperatures and in defining thermochemical transport systems. This report describes the development of an analytical model of an air and molten salt direct-contact heat exchanger.




---

Mark Bohn, Senior Engineer

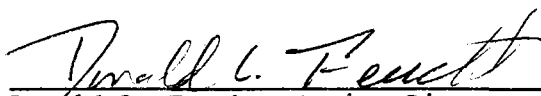
Approved for

SOLAR ENERGY RESEARCH INSTITUTE



---

David H. Johnson, Manager  
Thermal Sciences Research Branch



---

Donald L. Feucht, Acting Director  
Solar Heat Research Division

## SUMMARY

### Objective

To develop an analytical model that describes the heat transfer performance of a direct-contact heat exchanger operated as an irrigated packed bed at high temperature.

### Discussion

Direct-contact heat exchange can provide a cost-effective means of transferring heat between a gas and a liquid in applications where the gas and liquid do not react and can be separated after the heat exchange is effected. An especially attractive application is the production of high-temperature air from molten salt in a solar thermal central receiver system. The particular configuration of interest here is an irrigated packed bed in which the liquid is introduced at the top of a random bed of packing elements and flows in rivulets down the bed transferring heat to a counterflowing stream of gas. Experimental data and analytical models that describe the heat transfer performance of such a heat exchange device are lacking. This hampers efforts to determine the economic value of direct-contact heat exchange and to design commercial-sized systems.

In response to this problem, the present work was undertaken to provide an analytical model of direct-contact heat exchange. In addition to allowing commercial-sized design and comparison and extrapolation with experimental data, this model was developed to point out the important heat transfer mechanisms and to point the way to required future research. The model expands on existing models in that it uses the heat and mass transfer analogy and determines heat transfer at the gas-liquid interface via mass transfer correlations. Other modes of heat transfer, notably conduction in the bed packing, convection from dry portions of the packing to the gas, and radiation heat transfer, were added to the mass transfer correlations. Where available, correlations from the literature were used for calculating the contributions of the various heat transfer mechanisms.

### Conclusions

The model shows that radiation heat transfer is negligible (relative to the convective contributions) even at temperatures up to 1100°C and for large commercial-sized packing. This is consistent with available data at high temperature and simplifies the analysis considerably. The effect of variable properties can be handled in a simple manner. Comparing the resulting model with available data for a low-temperature oil and air system, we found that the model resulted in much better agreement with the data relative to previous models. Depending on the type of packing and how well it was wet by the liquid, the conduction in the packing has a relatively small effect but does tend to increase the heat-transfer rate predicted by the model closer to the data. Favorable agreement was also seen with an air and molten salt system, although little data were available for comparison. The model is not applicable to liquids that do not wet the packing because it relies on a wetting correlation developed for wetting liquids. For the air and molten salt system, it appears that we can achieve volumetric heat transfer coefficients of 6,000 to 12,000 W/m<sup>3</sup> °C.

## TABLE OF CONTENTS

	<u>Page</u>
1.0 Introduction.....	1
2.0 Heat Transfer Mechanisms.....	4
2.1 Convection at the Liquid-Air Interface.....	4
2.2 Convection Between the Gas and the Dry Packing Surface.....	8
2.3 Conduction in the Packing Element.....	9
2.4 Convection Between the Liquid Film and the Packing Surface.....	11
2.5 Radiation Among Portions of the Dry Packing and Conduction Among Packing Elements.....	13
2.6 Radiation Among Portions of the Liquid Film.....	14
2.7 Radiation Between the Liquid and Dry Packing Surface.....	14
3.0 Heat Transfer Equations.....	15
4.0 Results.....	21
5.0 Conclusions.....	27
6.0 References.....	28

**LIST OF FIGURES**

	<u>Page</u>
2-1 Correlation of (a) Gas-Side and (b) Liquid-Side Mass Transfer from Onda, Takeuchi, and Okumoto (1968).....	7
2-2 Packing Element with Liquid Film.....	10
2-3 Idealized Version of Packing Element with Liquid Film.....	10
3-1 Bed Schematic Used to develop Model.....	15
4-1 Comparison of Present Model with Results of Huang, $L = 2.71 \text{ kg/m}^2 \text{ s}$ , 1-in. Ceramic Raschig Rings.....	22
4-2 Comparison of Present Model with Results of Huang, $L = 2.71 \text{ kg/m}^2 \text{ s}$ , 1-1/2-in. Ceramic Raschig Rings.....	22
4-3 Comparison of Present Model with Results of Huang, $L = 2.71 \text{ kg/m}^2 \text{ s}$ , 1-in. Steel Pall Rings.....	22
4-4 Comparison of Present Model with Results of Huang, $L = 2.71 \text{ kg/m}^2 \text{ s}$ , 1-1/2-in. Steel Pall Rings.....	22
4-5 Comparison of Present Model with Results of Huang, $L = 2.71 \text{ kg/m}^2 \text{ s}$ , 1-in. Ceramic Intalox Saddles.....	23
4-6 Comparison of Present Model with Results of Huang, $L = 2.71 \text{ kg/m}^2 \text{ s}$ , 1-1/2-in. Ceramic Intalox Saddles.....	23
4-7 Comparison of Present Model with Results of Huang, $G = 1.34 \text{ kg/m}^2 \text{ s}$ .....	23
4-8 Comparison of Present Model with Results of Mackey and Warner (M&W), $L = 11.0 \text{ kg/m}^2 \text{ s}$ , 1/2-in. Carbon Raschig Rings.....	24
4-9 Comparison of the Present Model with Experimental Results for Air-Molten Carbonate Salt at 550°C, 5/8-in. Stainless Steel Pall Rings $L = 7.7 \text{ kg/m}^2 \text{ s}$ .....	25

**LIST OF TABLES**

3-1 Packing Specifications.....	17
3-2 Results of Packing Tests.....	18

## NOMENCLATURE

$a$	surface area per unit volume ( $m^{-1}$ )
$A_c$	cross section area of empty column ( $m^2$ )
$a_d$	dry surface area per unit volume ( $m^{-1}$ )
$A_f$	fin cross-sectional area ( $m^2$ )
$C_1$	constant in Eq. 2-4
$C_l$	liquid specific heat (J/kg K)
$C_p$	gas specific heat (J/kg K)
$D$	mass diffusivity ( $m^2/s$ )
$d_p$	characteristic packing dimension (m)
$d_{pw}$	packing diameter as defined by Whitaker, Eq. 2-7 (m)
$dQ$	local differential heat transfer in bed (W)
$dV$	incremental volume of bed ( $m^3$ )
$E$	$\exp(\lambda_1 - \lambda_2)$
$F$	defined in Eq. 2-21
$f_d$	fraction of dry surface area = $1 - a_w/a_p$
$F_{lp}$	view factor, liquid to packing
$Fr_l$	liquid-film Froude number $a_p L^2 / \rho_l^2 g$
$g$	acceleration of gravity ( $m/s^2$ )
$G$	gas loading = $\dot{m}_g / A_c$ ( $kg/m^2 s$ )
$h$	heat transfer coefficient ( $W/m^2 K$ )
$H_c$	column height (m)
$h_p$	height of the packing element (m)
$h_r$	radiation heat transfer coefficient ( $W/m^2 K$ )
$H_{tu}$	height of a transfer unit Eq. 3-9
$h_w$	heat transfer coefficient from Whitaker's correlation, Eq. 2-5 ( $W/m^2 K$ )
$k_c$	bed thermal conductivity (W/m K)
$k_g$	gas-side mass transfer coefficient ( $kg mol/h m^2 atm$ ); gas thermal conductivity (W/m K)
$k_l$	liquid-side mass transfer coefficient ( $m^3/s^3$ ); liquid thermal conductivity (W/m K)
$k_p$	thermal conductivity of packing (W/m K)



## NOMENCLATURE (Continued)

$k_{rb}$	effective-bed thermal conductivity, Eq. 2-17 (W/m K)
$k_{rl}$	liquid-to-liquid radiation thermal conductivity (W/m K)
$L$	liquid loading = $\dot{m}_l/A_c$ (kg/m <sup>2</sup> s)
$L_f$	fin length (m)
$m$	defined in Eq. 2-8 (m <sup>-1</sup> )
$\dot{m}$	mass flow rate (kg/s)
$M$	molecular weight (kg/kg mol)
$N_d$	number of fins per unit volume (m <sup>-3</sup> )
$N_R$	number of packing elements per unit volume (m <sup>-3</sup> )
$P$	fin perimeter (m); absolute pressure (atm)
$Pr$	Prandtl number
$Q_f$	fin heat transfer (W)
$q_{lpr}$	heat flux between liquid film and dry packing
$r$	droplet radius
$R$	gas constant (m <sup>3</sup> atm/K kg mol)
$Re_{ap}$	Reynolds number as defined by Whitaker, Eq. 2-6
$Re_{ff}$	falling-film Reynolds number, Eq. 2-12
$Re_g$	gas Reynolds number = $6G/a_p\mu_g$
$Re_l$	liquid-film Reynolds number = $L/a_p\mu_l$
$Sc_g$	Schmidt number
$T$	temperature (K)
$t_p$	thickness of packing material (m)
$Ua$	volumetric heat transfer coefficient (W/m <sup>3</sup> °C)
$V_p$	packing volume (m <sup>3</sup> )
$We_l$	liquid-film Weber number = $L^2/\rho_l\sigma a_p$
$x$	axial distance (m)
$\bar{x}$	dimensionless axial distance

## Greek

$\Gamma$	mass flow per unit width (kg/m s)
$\epsilon_l$	liquid emissivity

## NOMENCLATURE (Concluded)

$\epsilon_p$	packing emissivity
$\epsilon_v$	packing void fraction
$\theta$	dimensionless temperature
$\lambda_1, \lambda_2,$ $\lambda_3 \dots \lambda_7$	dimensionless parameters
$\mu$	viscosity (kg/m s)
$\rho$	density
$\sigma$	Stefan-Boltzman constant ( $W/m^2 K^4$ ); liquid surface tension (N/m)
$\sigma_c$	critical surface tension (N/m)

## Subscripts

d	droplet
e	effective
ff	falling film
g	gas
i	inlet
l	liquid
p	packing
r	radiative
lpr	liquid-to-packing, radiative
w	wet

**SERIO** 

## 1.0 INTRODUCTION

Direct contact is an important mechanism for transferring mass between one fluid stream and another in industrial processes. Examples of such processes include gas-liquid contacting for absorption, humidification, and stripping. Direct contact may also be used to effect heat transfer between two fluid streams, if that contact does not cause undesired chemical reactions and if the two streams can be separated afterwards. Direct-contact heat exchange (DCHX) is a potentially cost-effective method of transferring heat between such fluid streams primarily because it creates a very high surface area per unit volume. Additionally, intervening surfaces that exist for a conventional heat exchanger are not present. This increases the thermodynamic efficiency of the heat transfer process and further reduces the cost of the heat exchanger.

Because of the constraints on fluid stream compatibility, industry has exploited relatively few DCHX applications. One important exception is the heat transfer between molten salt and air in solar thermal central receiver applications. Here, the salt acts as a heat transfer fluid in the receiver and as a storage medium. DCHX can provide high-temperature air to an industrial process or to a turbine from the solar thermal energy stored in the salt. Conventional heat exchange technology uses a finned-tube heat exchanger. In a study of the comparative economics, Bohn (1985) showed that the direct-contact heat exchanger would be from 2 to 5 times more cost effective than a finned-tube exchanger, depending on the service temperature.

The particular DCHX configuration we are interested in is one in which counterflowing streams of a gas and a liquid enter a packed bed. As the liquid flows downward by gravity over the packing elements (rings, spheres, saddles, etc.), it is dispersed over the relatively large surface-area-per-unit volume of the packing element. Gas, flowing upward, contacts the liquid and the packing, and heat is transferred at the interface between the gas and liquid phases. In addition, radiation heat transfer may be important at high temperature.

This report presents a model for predicting the performance of such a heat exchanger, in particular at high temperatures and with emphasis on the air and molten salt system. An accurate and reliable DCHX model would allow commercial units to be designed with confidence and also allow new units to be scaled from existing ones. Developing such a model leads to a better understanding of the mechanisms of heat transfer and would allow us to differentiate between the important and unimportant mechanisms.

Of the many attempts to model problems involving direct-contact heat exchange, few have involved all aspects of this problem, namely simultaneous liquid and gas flow (irrigated bed), low-pressure-drop commercial packings, high-temperature operation, and molten salt working fluids with properties that differ substantially from liquids typically used in irrigated packed-bed experiments.

Balakrishnan and Pei (1979a,b) developed a model of heat exchange between a gas and spherical particles in a packed bed. Their model included conduction from sphere to sphere, convection to the gas, and radiation heat transfer from

sphere-to-sphere. The emphasis was on improving previous models for contact area: convection was included in an ad hoc way as a boundary condition at the sphere surface with a specified heat-transfer coefficient. The radiation component was calculated using known view factors for the given geometry of a packed bed of spheres. They concluded that radiation became significant at temperatures greater than 400 K for 0.635-cm-diameter spheres and that at 950 K the contributions of radiation and conduction were about equal.

Dixon (1985) modeled the thermal resistance of a packed bed with gas flow and used a simplified way to include radial terms. All heat-transfer mechanisms were lumped into effective thermal conductivities incorporated into a thermal network model. He did not consider radiation.

Huang (1982) presented experimental data on direct-contact heat exchange between air and mineral spirits for Raschig rings, Intalox saddles, Pall rings, and HyPak rings. The data were for temperatures in the range 30° to 50°C. He found that predicting the volumetric heat transfer from mass transfer data tended to be conservative, which he attributed to conduction heat transfer in the packing. Although this conduction effect was noted by other researchers, it was not incorporated into any heat transfer models.

Standish (1968) measured heat transfer between hot gases and mercury or cerrobend (a low-melting-point alloy) at low temperatures (up to 105°C) in an irrigated packed bed. He considered the direct heat transfer path from liquid to gas as well as the indirect path through the packing. Packings of higher thermal conductivity yielded higher volumetric heat transfer. Using cerrobend to wet the packing was more effective than using mercury, thus, the effect of packing thermal conductivity was less for the mercury. Standish did not attempt to experimentally separate the direct and indirect heat transfer contributions.

Mackey and Warner (1972) investigated a packed bed with counterflowing gas and liquid metals. They expressed the total heat transfer as the sum of three mechanisms: direct heat transfer between the liquid and gaseous phases, indirect heat transfer from liquid to gas via the packing, and radiation heat transfer. They did not attempt to model these mechanisms but rather to separate them experimentally. The direct component was determined from the heat-mass transfer analogy and mass transfer data for vaporizing mercury from the author's previous work. The indirect component could then be deduced from low-temperature experiments with mercury by subtracting out the direct heat transfer contribution. By then operating at high temperature with a low-vapor-pressure liquid metal (lead), they attempted to determine the radiation contribution by subtracting the direct and indirect effect from the overall effect. They considered the mercury system to be a low-temperature analog of the lead system. Their results indicated that the direct mechanism contributed 30% to 60% of the total heat exchange. For a packing with higher thermal conductivity (10-mm steel spheres) the indirect mechanism contributed about 67% of the total heat transfer compared with about 45% for lower thermal conductivity packing (1/2-in. carbon Raschig rings or 10-mm glass spheres). Thus, they also recognized the importance of conduction in the packing material. They did not find a significant effect of radiation in the 400°-600°C range; they report less than a 5% contribution to total heat transfer.

Although the work by Mackey and Warner would be useful for liquid metal-gas systems, it is not sufficiently general to apply to other systems. For example, their direct mechanism, which was estimated from mass transfer data, is not applicable to molten salts because salt-vapor mass-transfer coefficients have not been measured (because of their exceedingly low vapor pressures and because their vapors are unimportant to industry). Moreover, Mackey and Warner's equations for heat transfer do not allow us to determine when radiation would be important or why the different packing materials contributed differently to the direct and indirect mechanisms.

The model discussed here incorporates each heat-transfer mechanism individually rather than lumping them into an overall heat-transfer coefficient as done previously. Correlations available in the literature are used to calculate each heat-transfer rate; then, overall volumetric heat-transfer coefficients can be calculated. We have attempted to keep the model as general as possible; however, specific references to molten salt are required occasionally because of its unusual properties and our special interest in them.

## 2.0 HEAT TRANSFER MECHANISMS

The flow of liquid and gas in the packed bed was described qualitatively earlier, and that discussion makes it clear that modeling the heat transfer process involves several mechanisms:

1. Convection at the liquid-gas interface
2. Convection between the gas and the dry packing surface
3. Conduction in the packing element
4. Convection between the liquid and the packing surface on which it is flowing
5. Radiation among portions of the dry packing
6. Conduction among packing elements
7. Radiation among portions of the liquid film
8. Radiation from liquid to the packing.

Note that Mackey and Warner grouped 2, 3, 4, and presumably 7 in the indirect mechanism. Their direct mechanism corresponds to 1; 5, 6, and 7 correspond to their radiation mechanism.

Each heat transfer mechanism needs to be expressed on a volumetric basis. That is, those mechanisms that occur at a surface will be expressed as a product of a surface heat transfer coefficient and the surface area per unit volume over which the mechanism is active.

### 2.1 Convection at the Liquid-Air Interface

This mechanism represents heat transfer at the interface between liquid and gas in the bed. Thus, we need to know the interfacial surface area as well as the film coefficients on the liquid and on the gas side of the interface. Onda, Takeuchi, and Koyama (1967) developed a correlation that allows us to predict the fraction of packing area that will be wet by a liquid in a packed bed:

$$\frac{a_w}{a_p} = 1 - \exp \left[ -1.45 \text{Re}_l^{0.1} \text{Fr}_l^{-0.05} \text{We}_l^{0.2} \left( \frac{\sigma}{\sigma_c} \right)^{-0.75} \right]. \quad (2-1)$$

The Reynolds, Froude, and Weber numbers that appear in the correlation are based on liquid flow and liquid properties with the length scale being the inverse of the packing surface area per unit volume. The correlation depends on liquid flow, liquid properties (surface tension, viscosity, density), and properties of the packing, including surface area per unit volume and critical surface tension. Onda et al. used spheres, Raschig rings, and Berl saddles fabricated from ceramic, glass, and paper in sizes from 8 to 50 mm. A dye that stained the packing surface was added to the liquid (water, ethanol, glycerol, cane sugar) under study so they could estimate the wet surface area.

The correlation (Eq. 2-1) is valid over the range

$$\begin{aligned}0.04 < Re_{\ell} < 500 \\2.5 \times 10^{-9} < Fr_{\ell} < 1.8 \times 10^{-2} \\1.2 \times 10^{-8} < We_{\ell} < 0.27 \\0.3 < \sigma/\sigma_c < 2.0 .\end{aligned}$$

For the flow rates and properties of interest for molten carbonate salts on oxidized metal, this correlation yielded a wet surface area range of 40%-60%.

The critical surface tension is usually determined by measuring the contact angle of a homologous series of fluids of varying surface tensions on a given surface and then plotting the cosine of the contact angle versus the surface tension of the liquids. Liquids with low surface tension (e.g., ethanol) wet most surfaces and yield a low contact angle. Liquids with high surface tension (e.g., mercury) do not wet most surfaces and yield a contact angle close to 180 deg. Ellison and Zisman (1954) and Fox and Zisman (1952) present data that show a linear decrease of the contact angle cosine for increasing surface tension for a group of similar liquids in a given surface. Extrapolating the curve backwards to a zero contact angle yields the critical surface tension.

Onda, Takeuchi, and Koyama (1967) used a steel surface with a reported critical surface tension of 75 dyne/cm. The surface of interest for a molten salt application will likely be an oxidized metal or possibly alumina. Mamantov, Braunstein, and Mamantov (1981) and Moiseev and Stepanov (1967) report that the contact angle of the molten carbonate eutectic on oxidized metals is zero. This would imply that the critical surface tension for such a surface is greater than about 226 dyne/cm. We performed a semiquantitative test with ethanol, water, molten salt, and mercury on oxidized stainless steel. We found that although mercury ( $\sigma = 486$  dyne/cm) did not wet the surface, none of the other liquids completely wet the surface either so the curve (cosine of contact angle versus surface tension) was not as well defined as the theoretical plot. This is probably because the liquids used are not of a homologous group. Nonetheless, we have chosen the critical surface tension for the oxidized metal to be 300 dyne/cm because that is greater than the surface tension for molten salt (which has a very low or zero contact angle) but less than that for mercury, which exhibits a very large contact angle. As stated earlier, this correlation yielded a wet surface area range of 40%-60% for the flow rates and properties of interest for molten carbonate salts on oxidized metal.

While Onda's correlation predicts the fraction of packing surface wet by the liquid, Bravo and Fair (1982) point out that the actual surface area for mass transfer (and presumably heat transfer), known as the effective area  $a_e$ , must also include other contributions. These include the interfacial surface area provided by suspended and falling droplets, gas bubbles in liquid puddles, ripples on the liquid film surface, and any contribution caused by liquid film falling on the column wall. Others have found that the total holdup is effective in mass transfer (Mackey and Warner 1973) (probably because the mercury



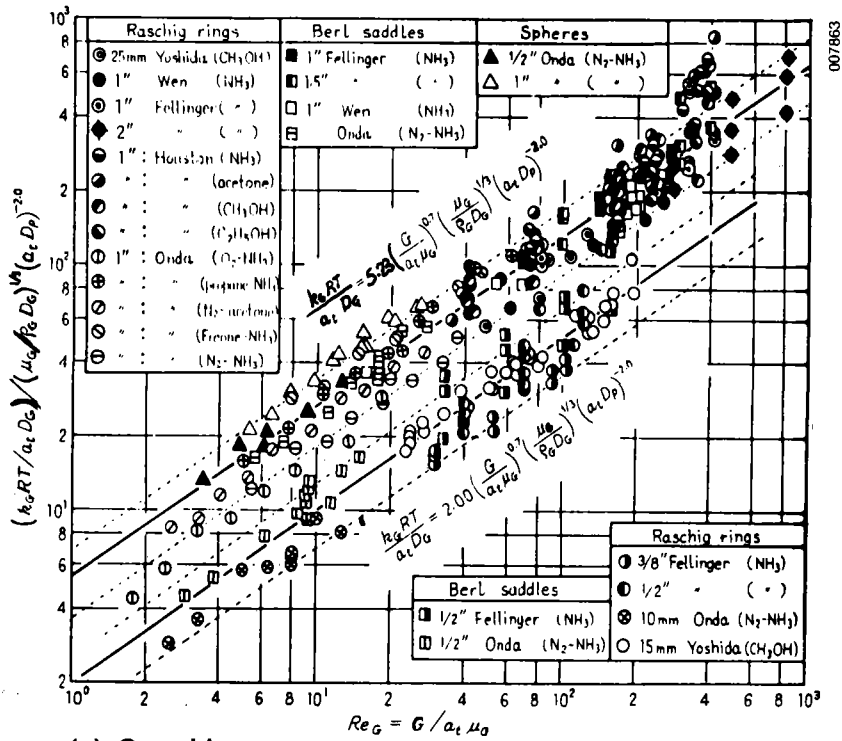
they used wet their packing very little, so interfacial area from the other sources would be important).

Like Onda's correlation for a wet surface area, Bravo and Fair's correlation for effective surface area was developed with liquids having a limited range of surface tension, e.g., 6 to 74 dyne/cm. Neither correlation has been validated for  $\sigma > \sigma_c$ , i.e., for nonwetting liquids. Using Bravo and Fair's correlation with typical flow and properties for air and molten salt systems, we found that it predicted effective areas about three times the packing surface area  $a_p$ , which seemed unreasonable. We also used the correlation to calculate  $a_e$  for Mackey and Warner's conditions with mercury and air and found that while Onda's correlation predicted wet surface areas of about 8%-28% of the packing area, Bravo and Fair's correlation predicted effective areas of about 100% of the packing area. The contribution of the droplets, gas bubbles, ripples, etc., to the interfacial surface area should increase this area beyond the wet area. However, such large increases seem unreasonable because they imply that the packing surface plays only a minor role in generating interfacial surface area and are not consistent with Mackey and Warner's flow visualization photographs. Since Onda's correlation at least gives wet surface areas that are within reason, we have chosen to use it as a basis for our model. However, keep in mind that it was developed for liquids with surface tension and viscosities considerably lower than molten salt.

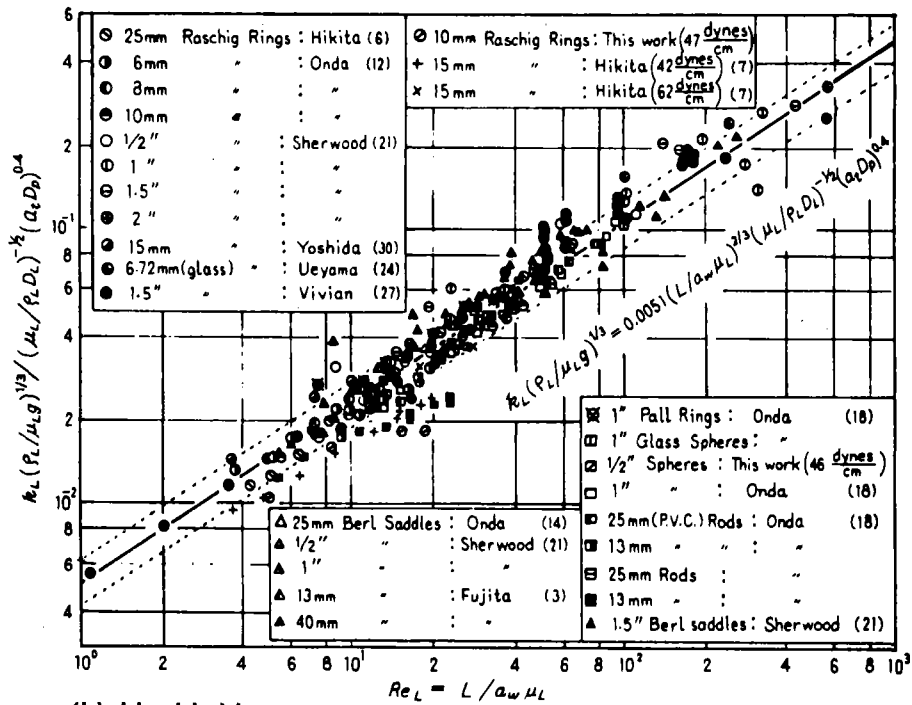
Because of a lack of heat transfer data or correlations that could be applied directly to the salt-air interfacial convection problem, we will follow others (Huang 1982, Fair 1972, and Bohn 1985) and apply the mass transfer-heat transfer analogy. We therefore require a mass transfer correlation to determine the heat transfer at the liquid-gas interface.

One such correlation is that of Onda, Takeuchi, and Okumoto (1968) that relies on the wet packing surface area developed by Onda, Takeuchi, and Koyama (1967), Eq 2-1, described previously. This mass transfer correlation was chosen for several reasons. Several researchers have found that Onda's model represents mass transfer data better than other available correlations. Bravo and Fair (1982) used Onda's mass transfer coefficient correlation in developing their general model based on effective mass transfer surface area. Kelly, Rousseau, and Ferrell (1984) used Onda's correlation in describing the physical absorption of acid gases in methanol partly because it was the only one of four correlations he considered that was based on packings as small as 0.25 in. In the end, Kelly found that only Onda's correlation allowed reasonably accurate design calculations.

The data used by Onda, Takeuchi, and Okumoto (1968) in developing his correlation are shown in Figure 2-1 and demonstrate one reason the correlation is successful. Onda used all available packing sizes, a wide range of flow rates, and several chemical systems in developing the correlation. The correlations are based on Raschig rings from 9.5 to 50 mm, spheres from 12.5 to 25 mm, and Berl saddles from 12.5 to 38 mm. Since Onda's correlation is based on data for a wide range of packing sizes, we anticipate that basing a heat transfer model on his correlation should also be satisfactory for all packing sizes. The liquids tested included methanol, ammonia, acetone, ethanol. Gases tested include oxygen, propane, nitrogen, and Freon.



(a) Gas-side



(b) Liquid side

Figure 2-1. Correlation of (a) Gas-Side and (b) Liquid-Side Mass Transfer from Onda, Takeuchi, and Okumoto (1968)

Onda's correlation also expresses the dimensionless mass transfer on the gas side (Figure 2-1a) as a function of gas Reynolds number, Prandtl number, and packing geometry; the correlation for the liquid side (Figure 2-1b) involves the liquid Reynolds number, Schmidt number, and packing geometry. Some other correlations in the literature present results in dimensional terms, which should cause concern for anyone trying to use the correlation for conditions different from those for which the correlation was derived.

The data for the gas side show a dependence on packing size with the data for the smaller packing falling lower than that for larger packing. Onda points out that for packing smaller than 15 mm, the leading coefficient decreases monotonically with  $a_p$ , and he recommends 2.0 as the leading constant  $C_1$  in the correlation Eq. 2-2<sup>p</sup> rather than 5.23. Figure 2-1b for the liquid side does not demonstrate this packing-size dependence. Note that even considering the two values of  $C_1$ , there is still considerable scatter, at least  $\pm 30\%$ .

The correlation equations for gas-side and liquid-side mass transfer coefficients are

$$k_g \left( \frac{RT}{a_p D_g} \right) = C_1 \left( \frac{Re_g}{6} \right)^{0.7} Sc_g^{1/3} (a_p d_p)^{-2}$$

$$k_l \left( \frac{\rho_l}{g \mu_l} \right)^{1/3} = 0.0051 \left( \frac{L}{a_w \mu_l} \right)^{2/3} Sc_l^{-1/2} (a_p d_p)^{0.4} \quad (2-2)$$

The constant  $C_1 = 2.0$  is for packing smaller than 15 mm, otherwise  $C_1 = 5.23$ .

Onda's mass transfer correlation equation may be used to predict heat transfer in the packed column from the mass transfer-heat transfer analogy, which relates dimensionless heat transfer and mass transfer coefficients on the gas side:

$$\frac{h_g a}{C_p G} = \left( \frac{Sc_g}{Pr_g} \right)^{2/3} \frac{k_g a_e P M_g}{G} \quad (2-3)$$

The power on the Schmidt number-Prandtl number ratio in Eq. 2-3 is 2/3 as recommended by Bravo and Fair (1982). Applying Eq. 2-3 to the Onda correlation, we find that for the dimensionless gas-side heat transfer coefficient:

$$\frac{h_g a}{C_p G} = \frac{C_1}{Pr_g^{2/3}} \frac{a_e a_p \mu_g}{G} \left( \frac{Re_g}{6} \right)^{0.7} (a_p d_p)^{-2} \quad (2-4)$$

In practice, the liquid-side film coefficient is about two orders of magnitude greater than the gas-side coefficient; therefore, we will neglect the liquid-side resistance. For molten salt flow rates and properties of interest, Eq. 2-4 gives volumetric heat transfer coefficients  $h_{gl}$  in the range of 2000 to 5000  $W/m^3 K$ .

**2.2 Convection Between the Gas and the Dry Packing Surface**

This mechanism represents the transfer of heat from dry portions of the packing to or from the gas. It is important because the liquid rivulets flowing

across the packing surface do not totally cover the packing surface area but yet can heat the dry areas. The mechanism here is transfer of heat from the liquid film to the packing and conduction through the packing material to the dry areas. The gas flowing over the dry areas can then transfer heat to the dry surface.

Convective heat transfer from dry packed beds has been studied extensively because of industrial interest in packed catalytic bed reactors, energy storage rock beds, and others. In these studies the main interest is the transfer of heat between the surface of the packing and the gas stream flowing over it. Whitaker (1972) has compiled data from five sources and developed a correlation applicable to the present problem:

$$\frac{h_w d_{pw}}{k_g} \left( \frac{\epsilon_v}{1 - \epsilon_v} \right) = Pr_g^{1/3} (0.5 Re_{ap}^{1/2} + 0.2 Re_{ap}^{2/3}) \quad (2-5)$$

for

$$10 < Re_{ap} < 10000 .$$

The Reynolds number is defined as

$$Re_{ap} = \frac{d_{pw} G}{\mu_g (1 - \epsilon_v)} . \quad (2-6)$$

The largest contribution of data to the correlation Eq. 2-5 is that of Taecker and Hougen (1949). They used Raschig rings from 6 to 50 mm. Other studies that provided data for Eq. 2-6 included cylinders and spheres. Note that the use of Eq. 2-5 neglects any effect on the heat transfer caused by interaction between the liquid film and the gas flowing over it.

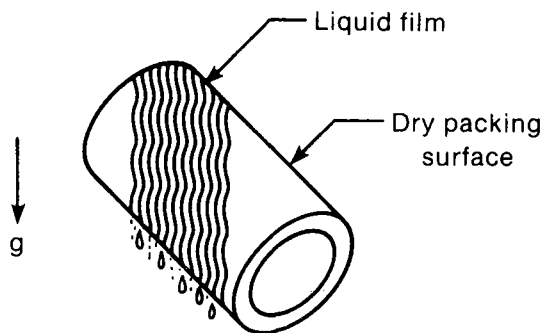
The packing diameter in Eq. 2-6 is defined as

$$d_{pw} = 6V_p/a_p . \quad (2-7)$$

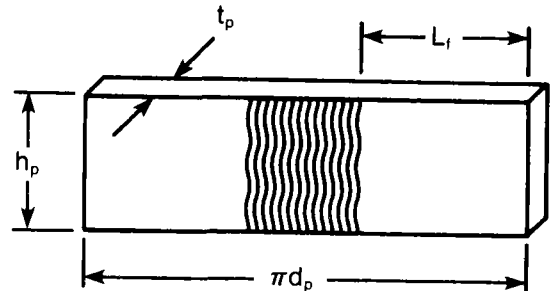
The packing volume  $V_p$  is defined as the volume of solid material comprising the packing. For a Raschig ring or a Pall ring of diameter  $d_p$ , height  $h_p$ , and made of a material of thickness of  $t_p$ , we have  $V_p = \pi d_p t_p h_p$ . The void fraction for the packing  $\epsilon_v$  is generally available as a property of the packing. For typical flow rates and property values, Eq. 2-5 gives local surface heat transfer coefficients of about  $70 \text{ W/m}^2 \text{ K}$ . If the packing were totally dry, this would be equivalent to a volumetric heat transfer coefficient of  $23,800 \text{ W/m}^3 \text{ K}$  for 5/8-in. Pall rings.

### 2.3 Conduction in the Packing Element

This heat transfer mechanism has been recognized by others as a possible reason why mass transfer correlations tend to underpredict heat transfer data. This is because conduction through the packing allows heat to transfer from wet areas to dry areas where the heat can subsequently be transferred to the gas stream. No comparable mechanism exists for mass transfer. To assess the magnitude of this effect and to determine if it can improve results calculated from mass transfer data, we developed a model based on conduction through and convection from a fin.



007867



007871

Figure 2-2. Packing Element with Liquid Film

Figure 2-3. Idealized Version of Packing Element with Liquid Film

Consider Figure 2-2, which depicts a packing element with liquid rivulets flowing down its surface. The flow of heat in the packing material and subsequent transfer to the surrounding gas flow is analogous to the transfer of heat from a body with fins to a gas flow. Heat is transferred from the root of the fin by conduction and then by convection to the gas stream. We will consider Figure 2-3 as an idealization of Figure 2-2 and will base our analysis of the packing conduction on this analogy to the fin effect.

An analysis of the fin effect is available in most heat transfer textbooks, Kreith and Bohn (1986), for example. Such an analysis gives the rate of heat transfer from each fin as

$$Q_f = (hPk_pA_f)^{1/2}(T_p - T_g) \tanh (mL_f) , \quad (2-8)$$

where

$$m = (hP/k_pA_f)^{1/2} .$$

To convert this expression to a volumetric basis, consider that the number of such fins per unit volume is

$$N_d = \frac{\text{dry surface area per unit volume}}{\text{dry surface area per fin}} = \frac{a_p - a_w}{L_f P} .$$

Since  $ha_{gp} = N_d q_f$ , we have

$$ha_{gp} = (hPk_pA_f)^{1/2} \tanh (mL_f) \left( \frac{a_p - a_w}{L_f P} \right) .$$

The heat transfer coefficient in Eq. 2-8 is that at the fin surface and therefore can be replaced by  $h_w$  from Eq. 2-5. The thermal conductivity is that of the packing material.

The fin perimeter  $P$ , heat flow cross-sectional area  $A_f$ , and fin length  $L_f$  require careful definition in the case of the partially wet packing element

for each type of packing. Looking at Figure 2-3, we see that the fin perimeter for the Raschig ring would be  $P = 2(t_p + h_p)$  if the ring is oriented with its axis vertical. If the ring axis is horizontal, we would have  $P = \pi d_p$ .

Since the rings are oriented randomly in the bed, we take the average of these two extremes, which gives us

$$P = \frac{1}{2}[2(t_p + h_p)\pi d_p] \quad \text{Raschig rings} \quad (2-9)$$

Similarly the heat flow cross-sectional area is

$$A_f = \frac{1}{2}(h_p t_p + \pi d_p t_p) \quad \text{Raschig rings} \quad (2-10)$$

where the two terms in parentheses are attributed to the vertical and horizontal ring orientations, respectively.

The fin length depends on how many rivulets are present on this packing surface. Idealize a vertically oriented Raschig ring with one rivulet, then the fin length would be  $(\pi d_p/2)f_d$ , and for a horizontal ring, we see that  $L_f = (h_p/2)f_d$ ; thus,

$$L_f = \frac{f_d}{4}(\pi d_p + h_p) \quad \text{Raschig rings} \quad (2-11)$$

For typical flow rates and properties consistent with those used previously to estimate heat transfer coefficients,  $h_{a,sp}$  will be  $8900 \text{ W/m}^3 \text{ K}$ . This reduction from  $23,800 \text{ W/m}^3 \text{ K}$  for the completely dry packed bed is because of a 50% reduction in dry surface area due to rivulets and the 75% fin efficiency for these conditions.

#### 2.4 Convection Between the Liquid Film and the Packing Surface

This mechanism involves the transfer of heat from the liquid film to the surface of the packing. A great deal of work has been done on falling film heat transfer primarily because of interest in condensers and in falling film evaporators.

Nusselt (1923) developed a theoretical model for heat transfer from laminar condensate films. This model was generally regarded as conservative after experimental data became available and Colburn (1934) improved it by including the effect of turbulence in the film. Bays and McAdams (1936) presented correlations of data for several liquids flowing in films on the inside of vertical pipes. Dukler (1960) sidestepped the issue of laminar versus turbulent flow in the film by numerically solving the equations of motion and energy for the problem using an eddy viscosity model for turbulence. Dukler's analysis also allows one to include the effect of shear at the gas-liquid interface; the effect is to further increase the heat transfer at the wall-liquid interface.

Relative to the present problem, any of these models will probably be conservative. This is because the models all consider a fully developed velocity field in the film while the film on the packing elements is being constantly interrupted. The velocity profile therefore must restart as the film begins to flow down from the top of each packing element. Nevertheless, all the

models predict very high surface heat transfer coefficients,  $O(2000 \text{ W/m}^2 \text{ K})$ . Coupled with the high wet surface area per unit volume, volumetric heat transfer coefficients of  $O(10^5 \text{ W/m}^3 \text{ K})$  result.

All the models present heat transfer as a function of film Reynolds number:

$$\text{Re}_{\text{ff}} = \frac{4\Gamma}{\mu_{\text{L}}}, \quad (2-12)$$

where  $\Gamma$  is the mass flow of liquid divided by the wet perimeter. This can be estimated from

$$\Gamma \cong \frac{L}{\pi d_{\text{p}}^2 N_{\text{R}} (a_{\text{w}}/a_{\text{p}})}, \quad (2-13)$$

yielding a Reynolds number of about 2.2 when  $L = 10 \text{ kg/m}^2 \text{ s}$ . For Reynolds numbers below about 1000, Dukler's analysis gives

$$h_{\text{ff}} \left( \frac{\mu_{\text{L}}^2}{\rho_{\text{L}}^2 g k_{\text{L}}^3} \right)^{1/3} = 0.36. \quad (2-14)$$

The effect of interfacial shear is negligible for these low Reynolds numbers. On a volumetric basis, then, we have

$$h_{\text{a}_{\text{Lp}}} = h_{\text{ff}} a_{\text{w}}. \quad (2-15)$$

The very high volumetric heat transfer coefficients indicate that the heat transfer from the liquid film to the packing is very effective. This is not surprising since the molten salt has a high thermal conductivity and the liquid film on the packing surface is thin. The results imply that the liquid is coupled indirectly to the air through conduction in the packing and by subsequent convection from dry areas to the air flow.

Since these correlations are valid for falling films, one must consider alternative correlations for applications in which the liquid does not wet the packing, e.g., mercury. McCormick and Baer (1963) determined the rate of droplet growth in dropwise condensation. From their expression of droplet growth, it is possible to determine the effective heat transfer coefficient at the droplet-condenser surface interface:

$$h_{\text{d}} = 4.15 k_{\text{L}} / r. \quad (2-16)$$

As an example, consider 0.25-mm-diameter mercury droplets, which are typical of those depicted in flow visualization photographs presented by Mackey and Warner (1973). This gives  $h_{\text{d}} = 137,000 \text{ W/m}^2 \text{ K}$ , or for a wet surface area of 8% (as predicted from Eq. 2-1) of the total packing area, we have a volumetric heat transfer coefficient of  $3.8 \times 10^6 \text{ W/m}^3 \text{ K}$ . We will make use of this correlation, Eq. 2-16, in Section 4.0 when analyzing Mackey and Warner's data.

## 2.5 Radiation Among Portions of the Dry Packing and Conduction Among Packing Elements

These two mechanisms exist even when the bed has no liquid or gas flowing through it. Mechanism 5 is the transfer of heat by radiation from one dry area on a packing element to another at different temperature. Mechanism 6 is the transfer of heat by conduction through the packing elements at a point of contact with other packing elements.

For simple geometric packing elements, e.g., spheres, it is possible to calculate the radiation component and the conduction component (Balakrishnan and Pei 1979a). This information can then be incorporated into one of two possible modeling techniques. In the first technique, the two-flux model (Larkin and Churchill 1959), the bed would be divided into small elements in the axial dimension, and flux entering (from adjoining elements) and flux leaving (because of scattering of the incoming radiation and reradiation) the element would be accounted for. The second technique is the effective thermal conductivity method. Here, the properties of the packed bed are used to calculate a thermal conductivity that, when multiplied by the local axial temperature gradient in the bed, yields the heat flux. The effective thermal conductivity method has been popular with those modeling radiation and conduction in dry packed beds (Young and See 1976, Kunii and Smith 1960).

The effective thermal conductivity technique is considerably simpler to implement for dimensional analysis purposes, and, as shown by Chen and Churchill (1963), it yields reasonably close results. (They attributed differences between their two-flux calculations and the effective thermal conductivity of Schotte [1960] to uncertainty in the emissivity of the packing, not to differences in the modeling techniques.) As we see shortly, precise estimates of the radiation-conduction terms are not necessary.

For complex packing elements, an exact analysis of the radiation between elements or packing-to-packing conduction is not possible. However, attempts have been made to calculate an effective thermal conductivity for Raschig rings with some success (Yagi and Kunii 1957). Their model involves thermal conductivities of the gas and solid, packing size, and three dimensionless length ratios. They found that at 700°C, the effective thermal conductivity of a bed of 9-mm ceramic Raschig rings was about 20 times that of air.

Schotte (1960) claimed that the model of Yagi and Kunii breaks down for small packing elements, and he presents an improved model for effective thermal conductivity:

$$k_{rb} = \frac{1 - \epsilon_v}{\frac{1}{k_p} + \frac{1}{h_r d_p}} + \epsilon_v h_r d_p + k_c, \quad (2-17)$$

where

$$h_r = 0.1952 \epsilon_p \frac{T_p^3}{106} \left( 1 - \frac{a_w}{a_p} \right). \quad (2-18)$$

The first term in Eq. 2-17 represents radiation to the packing in series with conduction through the packing, the second term represents radiation across



void spaces between the packing elements, and the third term represents the conduction component (to be taken from Figure 1 of Schotte). Using appropriate values for 1/2-in. Pall rings with an emissivity of 0.90 corresponding to oxidized steel, we find an effective thermal conductivity of 1.2 W/m K at 700°C, which compares very well with Yagi and Kunii's result of 20 times air conductivity for similar conditions.

**2.6 Radiation Among Portions of the Liquid Film**

Portions of the liquid film "see" other parts of the liquid film and thus may transfer heat by radiation. This may be calculated similarly to mechanism 5 without the conduction terms as derived by Schotte (1960):

$$k_{r\ell} = 0.1952d_p\epsilon_\ell \frac{T_\ell^3}{10^6} \frac{a_w}{a_p} . \tag{2-19}$$

**2.7 Radiation Between the Liquid and Dry Packing Surface**

Finally, the liquid film and dry portions of the packing surface see one another and exchange heat by radiation. Considering that the liquid film may only see other parts of the liquid film or dry packing surface areas, the heat flux exchanged by radiation between these two areas is

$$Q_{\ell pr} = \frac{\sigma(T_\ell^4 - T_p^4)}{F} , \tag{2-20}$$

where

$$F = \frac{1 - \epsilon_\ell}{\epsilon_\ell a_w} + \frac{1}{a_w F_{\ell p}} + \frac{1 - \epsilon_p}{\epsilon_p a_d} . \tag{2-21}$$

Because of the random nature of the liquid film flowing on the packing, it is not possible to calculate the liquid-to-dry packing view factor  $F_{\ell p}$ . Since the liquid may randomly appear anywhere in the field of view of an element of dry packing and vice versa, we equate  $F_{\ell p}$  with the fraction of dry surface area, or

$$F_{\ell p} = 1 - \frac{a_w}{a_p} . \tag{2-22}$$

The volumetric heat transfer coefficient for radiation heat transfer between the liquid film and the packing is then

$$ha_{\ell pr} = \frac{\sigma(T_\ell^4 - T_p^4)}{F(T_\ell - T_p)} . \tag{2-23}$$

Since the liquid film and the packing temperatures are close, this may be simplified to

$$ha_{\ell pr} = \frac{4\sigma T_\ell^3}{F} . \tag{2-24}$$

This is to be added to  $ha_{\ell p}$  (defined in Eq. 2-15), but for practical situations  $ha_{\ell pr} \ll ha_{\ell p}$  and may be neglected. From here on, we will have the symbol  $ha_{\ell p}$  be the sum of Eq. 2-15 and Eq. 2-24.

3.0 HEAT TRANSFER EQUATIONS

We incorporated the heat transfer mechanisms discussed in the previous section into a one-dimensional model in the dimension parallel to the liquid and gas flow. We considered pure counterflowing gas and liquid, i.e., no backmixing, and considered that three "continuous" phases exist in the bed: gas, liquid, and the packing. Further, we ignored radial heat losses out the column wall, assumed that the inlet gas and liquid temperatures were known, and assumed that the gas was transparent to radiation.

Figure 3-1 shows the packed bed in schematic. The bed is divided into elements of thickness  $\Delta x$  in the flow direction  $x$ . At the top of the element, liquid enters at temperature  $T_l(x+\Delta x)$  and gas exits at temperature  $T_g(x+\Delta x)$ . At the bottom of the element, liquid exits at temperature  $T_l(x)$  and gas enters at temperature  $T_g(x)$ . In the bed the average temperature of the packing is  $T_p(x)$ . The equation describing a heat balance on the liquid in element  $\Delta x$  is

$$\begin{aligned} \dot{m}_l C_l T_l(x + \Delta x) + k_{rl} A_c \frac{dT_l}{dx}(x + \Delta x) \\ + [T_g(x) - T_l(x)] h_{al} \Delta x A_c \\ + [T_p(x) - T_l(x)] h_{al} \Delta x A_c = \dot{m}_l C_l T_l(x) + k_{rl} A_c \frac{dT_l}{dx}(x) \end{aligned} \quad (3-1)$$

We neglected terms  $(\Delta x)^2$  and smaller. The first term is the enthalpy entering the element due to liquid flow, the second term is the flux entering the element due to radiation from the liquid above the element, the third term is the transfer of heat from the air to the liquid in the volume of bed within the element, and the fourth term is the transfer of heat from the packing to the liquid in the volume. The two terms on the right side of the equation represent the enthalpy leaving the element due to liquid flow and flux leaving

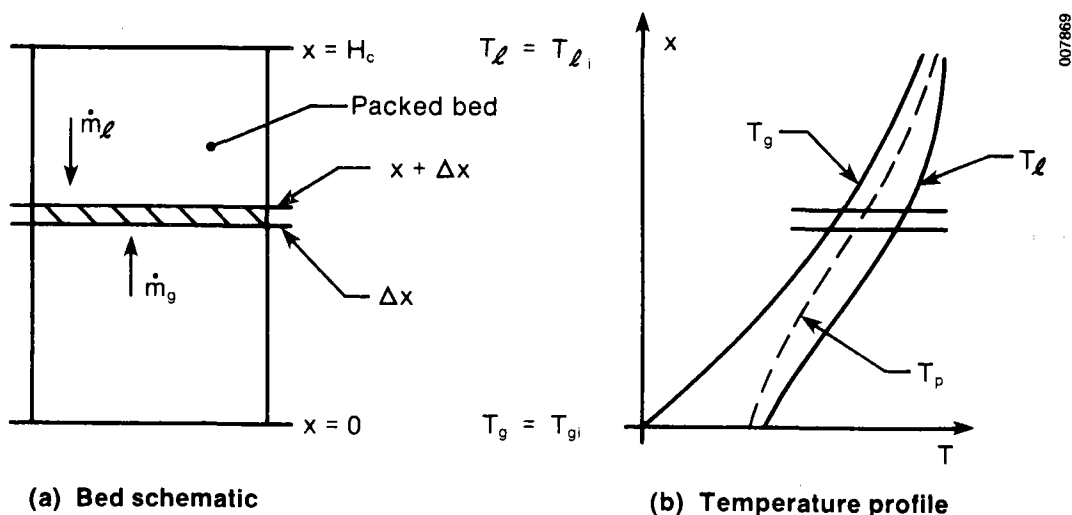


Figure 3-1. Bed Schematic Used to Develop Model

the element due to radiation to liquid below the element, respectively. The radiation terms are incorporated in the effective thermal conductivity  $k_{r\ell}$  and in  $ha_{\ell p}$  as the radiation from the liquid to the packing.

In the limit as  $dx \rightarrow 0$ , Eq. 3-1 becomes

$$LC_{\ell} \frac{dT_{\ell}}{dx} + k_{r\ell} \frac{d^2T_{\ell}}{dx^2} + (T_g - T_{\ell})ha_{\ell g} + (T_p - T_{\ell})ha_{\ell p} = 0 . \quad (3-2)$$

A similar equation expressing a heat balance on the gas in the element is

$$GC_{pg} \frac{dT_g}{dx} + (T_g - T_{\ell})ha_{\ell g} + (T_g - T_p)ha_{gp} = 0 . \quad (3-3)$$

The terms represent enthalpy caused by the gas mass flow, heat transfer to the liquid, and heat transfer to the packing, respectively. There are no radiation terms in the heat balance on the gas.

The equation expressing a heat balance on the packing is

$$k_{rb} \frac{d^2T_p}{dx^2} + (T_g - T_p)ha_{gp} + (T_{\ell} - T_p)ha_{\ell p} = 0 . \quad (3-4)$$

The terms represent heat flux caused by conduction and radiation out of the bed, heat transferred to the gas, and heat transferred to the liquid, respectively. The radiation terms are incorporated in the bed's effective thermal conductivity and in the radiation to the liquid in  $ha_{\ell p}$ .

These equations can be made dimensionless with the following scaling:

$$\begin{aligned} \tilde{x} &= x/H_c & \theta_g &= T_g/T_{\ell i} \\ \theta_{\ell} &= T_{\ell}/T_{\ell i} & \theta_p &= T_p/T_{\ell i} . \end{aligned}$$

The dimensionless form of the heat transfer equations then becomes

$$\begin{aligned} \frac{d^2\theta_{\ell}}{d\tilde{x}^2} + \lambda_1 \frac{d\theta_{\ell}}{d\tilde{x}} + \lambda_2(\theta_g - \theta_{\ell}) + \lambda_3(\theta_p - \theta_{\ell}) &= 0 \\ \frac{d\theta_g}{d\tilde{x}} + \lambda_4(\theta_g - \theta_{\ell}) + \lambda_5(\theta_g - \theta_p) &= 0 \\ \frac{d^2\theta_p}{d\tilde{x}^2} + \lambda_6(\theta_g - \theta_p) + \lambda_7(\theta_{\ell} - \theta_p) &= 0 . \end{aligned} \quad (3-5)$$

All the heat transfer coefficients, dimensions, flow rates, and property values were incorporated into seven dimensionless groups, which are

$$\begin{aligned} \lambda_1 &= \frac{LC_{\ell}H_c}{k_{r\ell}} = \frac{\text{enthalpy via liquid mass flux}}{\text{enthalpy via radiation}} \\ \lambda_2 &= \frac{ha_{\ell g}H_c^2}{k_{r\ell}} = \frac{\text{gas-liquid convection}}{\text{liquid-liquid radiation}} \end{aligned}$$

$$\lambda_3 = \frac{ha_{lp}H_c^2}{k_{rl}} = \frac{\text{liquid-packing convection/radiation}}{\text{liquid-liquid radiation}}$$

$$\lambda_4 = \frac{ha_{gl}H_c}{GC_{pg}} = \frac{\text{gas-liquid convection}}{\text{enthalpy via gas mass flux}}$$

$$\lambda_5 = \frac{ha_{gp}H_c}{GC_{pg}} = \frac{\text{gas-packing convection}}{\text{enthalpy via gas mass flux}}$$

$$\lambda_6 = \frac{ha_{gp}H_c^2}{k_{rb}} = \frac{\text{gas-packing convection}}{\text{packing radiation}}$$

$$\lambda_7 = \frac{ha_{lp}H_c^2}{k_{rb}} = \frac{\text{liquid-packing radiation and convection}}{\text{packing radiation}}$$

The magnitude of the seven dimensionless groups was determined by using the previously discussed correlations for  $k_{rl}$ ,  $ha_{lg}$ , etc., for three cases: (1) conditions typical of an experimental-sized DCHX with air and molten carbonate salt at 500°C, (2) conditions typical of a commercial-sized DCHX with air and molten carbonate salt at 900°C, and (3) conditions typical of an advanced commercial-sized DCHX operating at 1100°C. For case 3 the choice of materials is unknown, so we will assume that the salt has similar properties to the carbonate salt as used for cases 1 and 2 and that the packing has properties similar to high purity alumina. Note that the larger, more open, 2-in. rings should allow more radiative heat transfer in the bed. We will operate each case so the pressure drop is a nominal 1/2 in./ft (water column), which is a typical packed-bed operating condition. Table 3-1 identifies details of the three cases. Results are presented in Table 3-2.

At higher temperatures, the packing is fully wet. This is because of the reduced salt viscosity. With little or no dry area,  $ha_{gp}$  is negligible. The heat transfer at the salt and air interface does not change much with temperature. The bed radiative thermal conductivity  $k_{rb}$  is reduced for the higher temperature cases, again because there is very little dry surface for radiative interchange. The radiative conductivity that does increase with temperature is the salt-salt radiative conductivity  $k_{rl}$ . This is because of the larger wet area and the higher average salt temperature.

Table 3-1. Packing Specifications

Packing	Case 1 1/2-in. steel Pall rings, oxidized	Case 2 2-in. Inconel Pall rings, oxidized	Case 3 2-in. alumina Pall rings
Column height (m)	0.61	5.0	5.0
Salt flow (kg/m <sup>2</sup> s)	10.7	20.0	20.0
Salt inlet (°C)	500	900	1100
Gas flow (kg/m <sup>2</sup> s)	1.07	1.87	1.87
Gas inlet (°C)	450	700	700

Table 3-2. Results of Packing Tests

	Case 1	Case 2	Case 3
$ha_{lg}$	3165	3364	3364
$ha_{lp}$	$4.9 \times 10^5$	$1.1 \times 10^6$	$1.1 \times 10^6$
$ha_{gp}$	9349	5.9	5.9
$k_{rb}$	0.95	0.23	0.23
$k_{rl}$	0.60	14.5	23.6
$a_w/a_p$	0.45	0.99	0.99
$\lambda_1$	$1.9 \times 10^4$	$1.4 \times 10^4$	$0.8 \times 10^4$
$\lambda_2$	$1.9 \times 10^3$	$5.8 \times 10^3$	$3.6 \times 10^3$
$\lambda_3$	$3.0 \times 10^5$	$1.9 \times 10^6$	$1.2 \times 10^6$
$\lambda_4$	1.6	7.6	7.6
$\lambda_5$	4.9	0.13	0.13
$\lambda_6$	$3.7 \times 10^3$	$6.4 \times 10^2$	$6.4 \times 10^2$
$\lambda_7$	$1.9 \times 10^5$	$1.2 \times 10^8$	$1.2 \times 10^8$

Considering the values of  $\lambda$  for case 1, we see that all those with radiative terms in the denominator are very large. This means that the heat transfer caused by salt-air convection, salt-packing convection, and air-packing convection and enthalpy transfer caused by salt and air flow are much larger than heat transfer due to the radiative mechanisms. Only  $\lambda_4$  and  $\lambda_5$  are  $O(1)$ , meaning that the convective terms are the same order as the enthalpy flux terms. From this we would conclude that the radiative heat transfer mechanisms are not important because the convective heat transfer coefficients are very large.

The same observation holds true for the higher temperature cases. We note that the  $\lambda$ , which involve the air-packing terms ( $\lambda_5$  and  $\lambda_6$ ), are smaller than in case 1; but since the air-packing convection is not important for these cases due to a fully wet packing, the observation that radiation is not important still holds. This is very significant because it means that in commercial applications, even at the highest temperatures likely to be encountered, radiation heat transfer is not important relative to the convective mechanisms. This conclusion is different from the dry packed bed where the very large liquid convection terms are absent and the radiative terms must be retained.

Without the radiative terms, the equations simplify considerably. Namely, we are left with three coupled first-order linear differential equations of the form:

$$\lambda_1 \theta_l' + \lambda_2 (\theta_g - \theta_l) + \lambda_3 (\theta_p - \theta_l) = 0 \quad (3-6a)$$

$$\theta_g' + \lambda_4(\theta_g - \theta_l) + \lambda_5(\theta_g - \theta_p) = 0 \quad (3-6b)$$

$$\lambda_6(\theta_g - \theta_p) + \lambda_7(\theta_l - \theta_p) = 0, \quad (3-6c)$$

where

$$\theta' \equiv \frac{d\theta}{d\tilde{x}}.$$

Eq. 3-6c can be eliminated, yielding two coupled equations

$$\lambda_1 \theta_l' + \lambda_2(\theta_g - \theta_l) + \lambda_3 \left( \frac{\lambda_6}{\lambda_7 + \lambda_6} \right) (\theta_g - \theta_l) = 0 \quad (3-7)$$

$$\theta_g' + \lambda_4(\theta_g - \theta_l) + \lambda_5 \left( \frac{\lambda_7}{\lambda_7 + \lambda_6} \right) (\theta_g - \theta_l) = 0$$

with the boundary conditions

$$\theta_g(0) = \theta_{gi} \quad \text{and} \quad \theta_l(1) = 1.$$

If the property values and hence  $\lambda$ 's can be assumed to be constant, these equations can be solved exactly. To confirm that property value variation did not significantly affect the results, we first solved Eq. 3-7 with variable properties. This was accomplished with the shooting method; i.e., we guessed at  $\theta_l(0)$  and solved Eq. 3-7 using a forward difference scheme from  $x = 0$  to  $x = 1$ . By adjusting the guess for  $\theta_l(0)$ , we eventually converged on the correct solution, which required that  $\theta_l(1) = 1$ . Property values were calculated for air and for the carbonate salt at each step in the finite difference calculation. We tested this procedure against a constant property solution and found that if we used the property values calculated at the mean temperature for each stream as the constant property, the solution was very close to the variable property calculation.

Without the radiation terms and assuming constant properties, Eq. 3-7 simply describes heat transfer in a counterflow heat exchanger. It is a straightforward procedure to solve the equations if needed. However, the volumetric heat transfer coefficient can be extracted from the differential equations with

$$Ua = \frac{dQ}{dV} \frac{1}{T_l - T_g} = T_{li} \frac{LA_c C_l}{H_c} \frac{d\theta_l}{d\tilde{x}}.$$

Equation 3-7 may be manipulated to give an expression for  $d\theta_l/d\tilde{x}$ , resulting in

$$Ua = ha_{gl} + \frac{ha_{gp} ha_{lp}}{ha_{gp} + ha_{lp}}. \quad (3-8)$$

Equation 3-8 simply states that the overall heat transfer coefficient is composed of the liquid-gas thermal resistance in parallel with the series combination of the liquid-packing resistance and the gas-packing resistance. Since we found that  $ha_{lp}$  is very large, Eq. 3-8 simplifies to  $Ua = ha_{gl} + ha_{gp}$ . However, we will retain the more general form, Eq. 3-8. The results may also be expressed in terms of the height-of-a-transfer unit if desired:

$$H_{tu} = \frac{GC_p}{U_a} . \quad (3-9)$$

To meet the requirement that the average of the inlet and outlet temperatures for each fluid stream be used to calculate the fluid properties, an iterative solution was used. Results can be given as either  $U_a$  or  $H_{tu}$  as a function of  $G$ ,  $L$ ,  $T_{2i}$ , and fluid and packing properties.

#### 4.0 RESULTS

A comparison of the results of the present model with that of Huang (1982) along with Huang's data are shown in Figures 4-1 through 4-7. In Figures 4-1 through 4-6 the volumetric heat transfer coefficient  $Ua$  is plotted against  $G$  with  $L$  held constant. In all these plots we see that the results for  $ha_{lg}$  (the convective heat transfer at the liquid-gas interface to be compared with Huang's model) consistently agree better with Huang's data than Huang's model, even though the derivation for both models is based on the mass transfer analogy. We attribute the difference to our usage of a  $2/3$  power on the Schmidt-Prandtl number ratio in the mass transfer-heat transfer analogy while Huang used a  $1/2$  power. Note, however, that neither model appears to exhibit the same slope as the data, and this suggests a more fundamental problem with using mass transfer data to predict heat transfer for packed beds.

For all three types and two sizes of packing (ceramic Raschig rings, carbon steel pall rings, and ceramic Intalox saddles, 1-in. [not shown here] and 1-1/2-in. sizes) the correction for conduction (see curve labeled  $Ua$ ) in the packing further improves the agreement with the data. Generally, this correction is fairly small because the wet areas are a large fraction of the total packing area. Wet areas ranged from 80% to 90% of the packing area. Since the conduction correction is applied only over the dry area, the increase in heat transfer area is small, e.g., 10% to 20% of the packing area. The correction for the Intalox saddles is the largest because the saddles exhibit the smallest wet area, 80% to 82%. The correction for the Pall rings is the smallest because they exhibit the largest wet area, 86% to 90%.

A comparison of the data and models at fixed  $G$  and variable  $L$  is shown in Figure 4-7. Similar conclusions can be drawn here; e.g., the models do not predict the same sensitivity to  $L$  as do the data, general agreement is fairly good, and the present model with the conduction correction is an improvement over the original model by Huang (1982).

Comparison of the model results with Mackey and Warner's experimental results (1972) is a relatively severe test because their use of mercury minimized wetting of the packing. Since our main interest is in applications where the packing is well wet, comparison of the model results with nonwetting data is mostly of academic interest. It was pointed out earlier that for nonwetting liquids, the use of a drop-wise condensation model for the heat transfer between the liquid and the packing was more sensible than a falling film model. However, since we found that

$$ha_{lp} \gg ha_{gp}$$

for either the drop-wise or the falling-film model, we have simply

$$Ua = ha_{gl} + ha_{gp} ,$$

and the choice of model for  $ha_{lp}$  is immaterial.



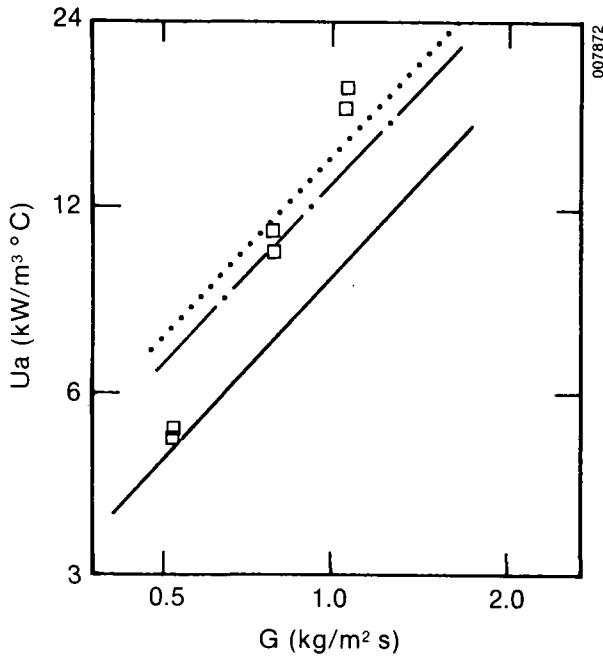


Figure 4-1. Comparison of Present Model with Results of Huang,  $L = 2.71 \text{ kg/m}^2 \text{ s}$ ,  $\square$  Huang data, — Huang Model for  $h_{a,lg}$ , - - - Present Model for  $h_{a,lg}$ , ..... Present Model for  $U_a$ , 1-in. Ceramic Raschig Rings

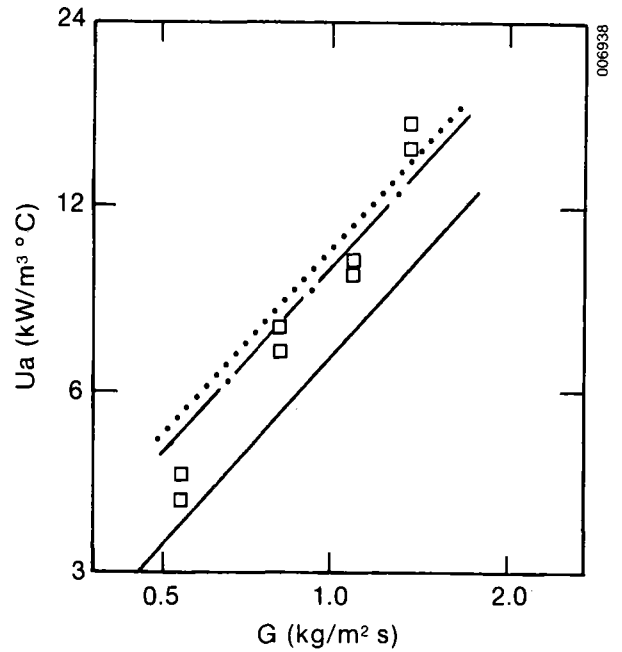


Figure 4-2. Comparison of Present Model with Results of Huang,  $L = 2.71 \text{ kg/m}^2 \text{ s}$ ,  $\square$  Huang data, — Huang Model for  $h_{a,lg}$ , - - - Present Model for  $h_{a,lg}$ , ..... Present Model for  $U_a$ , 1-1/2-in. Ceramic Raschig Rings

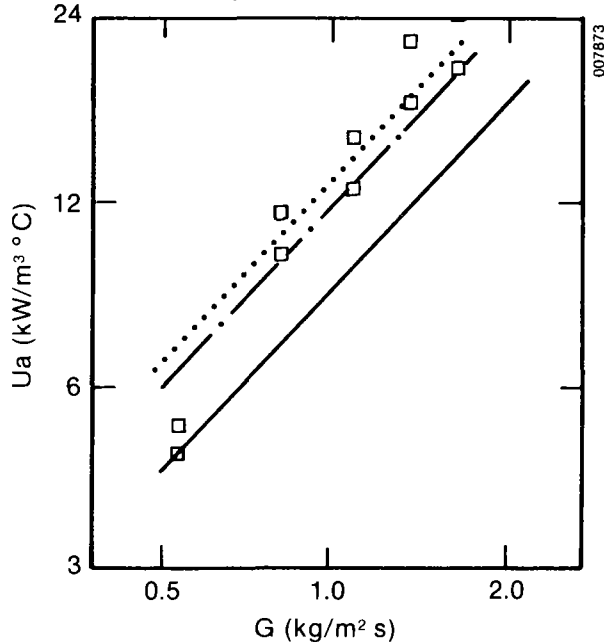


Figure 4-3. Comparison of Present Model with Results of Huang,  $L = 2.71 \text{ kg/m}^2 \text{ s}$ ,  $\square$  Huang data, — Huang Model for  $h_{a,lg}$ , - - - Present Model for  $h_{a,lg}$ , ..... Present Model for  $U_a$ , 1-in. Steel Pall Rings

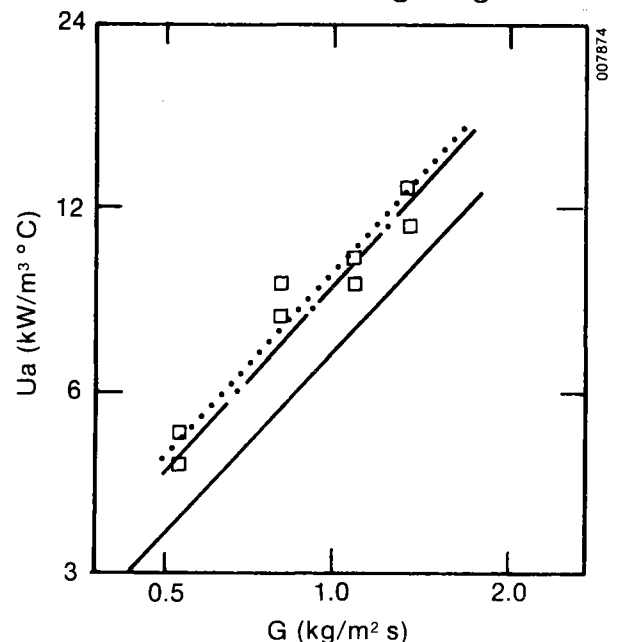


Figure 4-4. Comparison of Present Model with Results of Huang,  $L = 2.71 \text{ kg/m}^2 \text{ s}$ ,  $\square$  Huang data, — Huang Model for  $h_{a,lg}$ , - - - Present Model for  $h_{a,lg}$ , ..... Present Model for  $U_a$ , 1-1/2-in. Steel Pall Rings

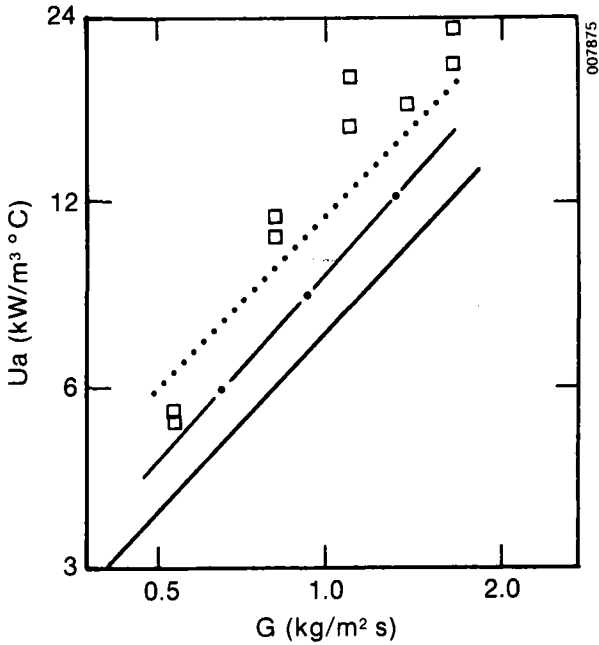


Figure 4-5. Comparison of Present Model with Results of Huang,  $L = 2.71 \text{ kg/m}^2 \text{ s}$ ,  $\square$  Huang data, — Huang Model for  $h_{a,lg}$ , — . — Present Model for  $h_{a,lg}$ , ..... Present Model for  $U_a$ , 1-in. Ceramic Intalox Saddles

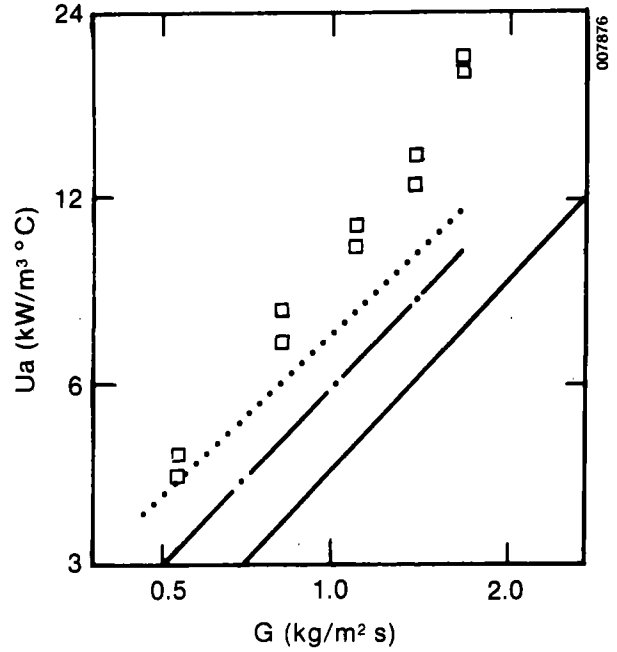


Figure 4-6. Comparison of Present Model with Results of Huang,  $L = 2.71 \text{ kg/m}^2 \text{ s}$ ,  $\square$  Huang data, — Huang Model for  $h_{a,lg}$ , — . — Present Model for  $h_{a,lg}$ , ..... Present Model for  $U_a$ , 1-1/2-in. Ceramic Intalox Saddles

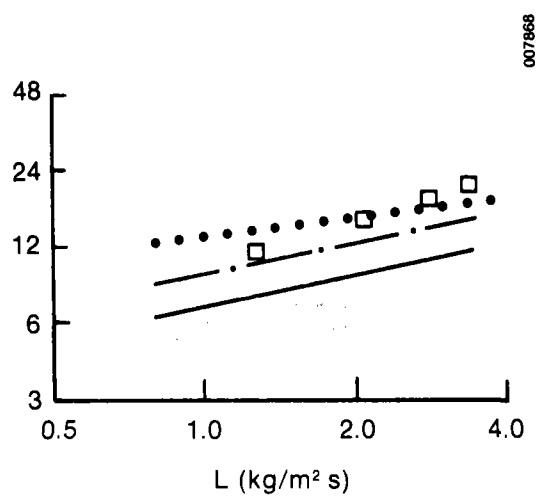
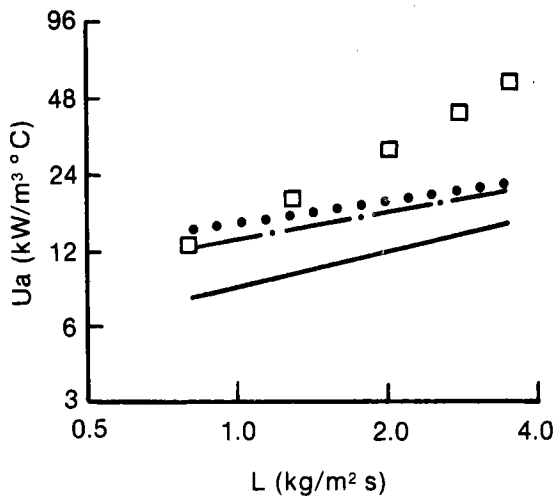


Figure 4-7. Comparison of Present Model with Results of Huang,  $G = 1.34 \text{ kg/m}^2 \text{ s}$ ,  $\square$  Huang data, — Huang Model for  $h_{a,lg}$ , — . — Present Model for  $h_{a,lg}$ , ..... Present Model for  $U_a$ . Left-hand figure is for 1-in. ceramic Raschig rings, right-hand figure is for 1-in. ceramic Intalox saddles.

A problem with the comparison of interest here is determining the critical surface tension  $\sigma_c$ . For the mercury system, which is nonwetting, we have  $\sigma_c < \sigma$ , but very little additional information is available. Thus, we have chosen to use  $\sigma_c$  as a parameter for the comparison. The upper limit to  $\sigma_c$  is  $\sigma = 484$  for mercury.

Figure 4-8 expresses the results in terms of the height-of-a-transfer unit vs. gas Reynolds number. Good agreement of the present model for  $ha_{gl}$  with the Mackey and Warner measurement of the direct component is seen for  $\sigma_c = 300$  to 400 N/m. This range of critical surface tension produces wet surface areas from 27% to 32%, which seems somewhat high by comparison with Mackey and Warner's flow visualization photograph. As a result, the fin effect correction is too large, producing  $H_{tu}$  about half that of Mackey and Warner's experimental data for combined direct and indirect heat transfer.

Using a lower critical surface tension of  $\sigma_c = 100$  N/m produces wet areas of 13%, which is more consistent with Mackey and Warner's visualization photograph. However, we then have  $\sigma/\sigma_c < 0.3$ , which is outside the range of applicability of Eq. 2-1. Therefore, we conclude that since Onda's wetting correlation, Eq. 2-1, was not tested for very high surface tension liquids, its applicability and the applicability of the present model is limited to lower surface tension liquids, specifically those that wet the packing surface.

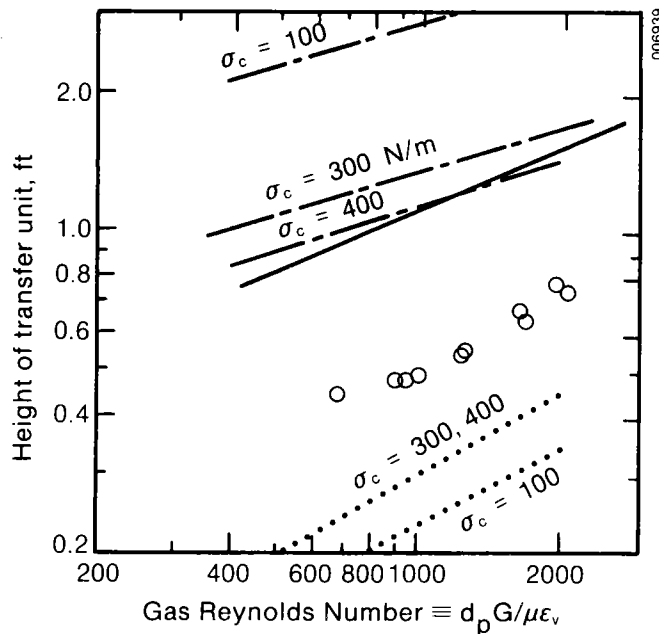


Figure 4-8. Comparison of Present Model with Results of Mackey and Warner (M&W),  $L = 11.0 \text{ kg/m}^2 \text{ s}$ .  $\circ$  M&W data, — M&W Direct Component, — — Present Model for  $ha_{gl}$ , ..... Present Model for  $Ua$ , 1/2-in. Carbon Raschig Rings.

Another important conclusion from Mackey and Warner's data is that the effect of radiation is negligible. Mackey and Warner compared results from the room temperature air and mercury system with results from their lead and nitrogen system at 450°C and found that  $U_a$  varied by less than 5% for this large temperature change. Thus, consistent with the analysis presented here, radiation heat transfer does not play an important role in an irrigated packed bed DCHX.

Finally, we wish to report on preliminary measurements of  $U_a$  in an air and molten salt system at 550°C performed as a part of the work presented in this paper. A more detailed discussion of the experimental apparatus will be presented in the near future.

Measurements were made in a 0.152-m inside diameter packed column, 0.61-m bed height. The packing was oxidized 5/8-in. stainless steel Pall rings, and the salt was the eutectic of lithium-sodium-potassium carbonate (43.5%, 31.5%, 25.0%, molar, respectively), which melts at 397°C. Preheated air at about 450°C was supplied by an electric air heater at the base of the column and distributed uniformly to the bed base. Salt was distributed by a three-hole canister-type liquid distributor that, in turn, was fed from a single salt inlet pipe.

Our previous experience indicated that measuring  $U_a$  from the terminal air and salt temperatures is exceptionally difficult and leads to conservative estimates of  $U_a$  (Bohn 1985). This is primarily because the air outlet temperature and the salt inlet temperature are very close, and small errors (caused by two-phase flow and radiation) produce large errors in the log-mean temperature used to calculate  $U_a$ . To avoid this difficulty in the present experiments, we measured the salt temperature distribution in the packed bed with thermocouples designed to sense only the molten salt temperature. According to the model presented herein, this temperature distribution should be exponential in axial distance through the bed. Fitting the measured bed salt temperatures to an exponential curve yields the volumetric heat transfer coefficient. Typically, the correlation coefficients for these curve fits are 0.95 or better.

Results are presented in Figure 4-9 for experimental points at fixed liquid rate and three air rates. Comparison with the model shows very good agreement for two of the points (better than 6%) and reasonable agreement with one point (better than 24%). The range of air flow tested here covers a large fraction of the actual column working range. It would be useful to test a range of liquid flow rates, although based on our previous work and results of others,  $L$  has a fairly weak effect on  $U_a$ . We also intend to test a range of

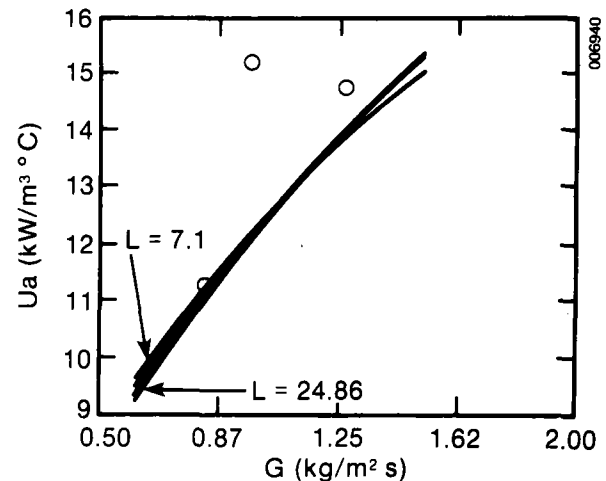


Figure 4-9. Comparison of the Present Model with Experimental Results for Air-Molten Carbonate Salt at 550°C, 5/8-in. Stainless Steel Pall Rings.  $\circ$  Experimental Data, — Model Results,  $L = 7.7 \text{ kg/m}^2 \text{ s}$ .

temperatures to confirm a lack of effect of radiation heat transfer. Nevertheless, this preliminary set of data seems to confirm that the model can predict with reasonable accuracy heat transfer in an irrigated packed column DCHX. It is also important to note that the measured and predicted volumetric heat transfer coefficients are about 3 to 4 times larger than we measured earlier because of the previously mentioned experimental difficulties (Bohn 1985). Since our previous work concluded that DCHX was a very cost-effective technology for heating gases with liquids, results presented herein reinforce this conclusion and, in fact, show that DCHX is even more cost effective than previously thought.

## 5.0 CONCLUSIONS

We have presented a model of direct-contact heat exchange in an irrigated, packed bed operating at high temperatures. All modes of heat exchange were accounted for in the model, and each was modeled with correlations available in the literature. Most of these correlations have been thoroughly tested and are based on a wide range of packing sizes, so we expect the model to be applicable to commercial-sized heat exchangers. A dimensionless analysis reveals that for such systems operating even at the highest reasonable temperatures, radiation heat transfer is not important compared with the convective terms in the equations. The model also includes, in an explicit manner, the packing conduction effect recognized by several researchers but not previously modeled.

The unimportance of radiation heat transfer is confirmed by data available in the literature. Comparison of the model with literature data also indicates that our model predicts the experimental data more accurately than do other models, and that the correction for packing conduction further improves the comparison with the data. Generally, the resulting model fits the data within experimental scatter, although note that none of the mass-transfer-analogy base models predict the sensitivity of  $U_a$  to  $L$  or  $G$  accurately. This suggests a fundamental problem with using the analogy even though results of sufficient accuracy for engineering purposes seem possible. Usage of the model is not recommended for liquids that do not wet the packing. Finally, comparison with experimental data for air and molten salt data at high temperatures indicates good agreement with the model for at least a restricted range of liquid flow rates.

## 6.0 REFERENCES

- Balakrishnan, A. R., and D. C. T. Pei, 1979a, "Heat Transfer in Gas-Solid Packed Bed Systems. 2. The Conduction Mode," Industrial & Engineering Chemistry Process Design and Development, Vol. 18, No. 1, pp. 40-46.
- Balakrishnan, A. R., and D. C. T. Pei, 1979b, "Heat Transfer in Gas-Solid Packed Bed Systems. 3. Overall Heat Transfer Rates in Adiabatic Beds," Industrial & Engineering Chemistry Process Design and Development, Vol. 18, No. 1, pp. 47-50.
- Bays, G. S., Jr., and W. H. McAdams, 1936, "Heat Transfer Coefficients in Falling Film Heaters," Industrial & Engineering Chemistry, Vol. 29, No. 11, pp. 1240-1246.
- Bohn, M., 1985, "Air/Molten Salt Direct Contact Heat-Transfer," Journal of Solar Energy Engineering, Vol. 197, pp. 208-214.
- Bravo, J. L., and J. R. Fair, 1982, "Generalized Correlations for Mass Transfer in Packed Distillation Columns," Industrial & Engineering Chemistry Process Design and Development, Vol. 21, pp. 162-170.
- Chen, J. C., and S. W. Churchill, 1963, "Radiant Heat Transfer in Packed Beds," AIChE Journal, Vol. 9, No. 1, pp. 35-41.
- Colburn, A. P., 1934, Transactions of American Institute of Chemical Engineers, Vol. 30, pp. 187.
- Dixon, A. G., 1985, "Thermal Resistance Models of Packed-Bed Effective Heat Transfer Parameters," AIChE Journal, Vol. 31, No. 5, pp. 826-834.
- Dukler, A. E., 1960, "Fluid Mechanics and Heat Transfer in Vertical Falling-Film Systems," Chemical Engineering Progress, Symposium Series, Vol. 56, No. 30, pp. 1-10.
- Ellison, A. H., and W. A. Zisman, 1954, "Wettability of Halogenated Organic Solid Surfaces," Journal of Physical Chemistry, Vol. 58, pp. 260-265.
- Fair, J. R., 1972(June) "Designing Direct Contact Coolers/Condensers," Chemical Engineering, pp. 91-100.
- Fox, H. W., and W. A. Zisman, 1952, "The Spreading of Liquids on Low-Energy Surfaces. III. Hydrocarbon Surfaces," Journal of Colloid Science, Vol. 7, pp. 428-442.
- Huang, C., 1982, "Heat Transfer by Direct Gas-Liquid Contacting," M.S. Thesis, Austin, TX: University of Texas.
- Kelly, R. M., R. W. Rousseau, and J. K. Ferrell, 1984, "Design of Packed, Adiabatic Absorbers: Physical Absorption of Acid Gases in Methanol," Industrial & Engineering Chemistry Process Design and Development, Vol. 23, pp. 102-109.

- Kreith, F., and M. S. Bohn, 1986, Principles of Heat Transfer, 4th Ed., New York: Harper and Row.
- Kunii, D., and J. M. Smith, 1960, "Heat Transfer Characteristics of Porous Rocks," AIChE Journal, Vol. 6, No. 1, pp. 71-78.
- Larkin, B. K., and S. W. Churchill, 1959, "Heat Transfer by Radiation Through Porous Insulations," AIChE Journal, Vol. 5, No. 4, pp. 467-474.
- Mackey, P. J., and N. A. Warner, 1972, "Heat Transfer Between Dispersed Liquid Metals and Gases in Packed Beds," Metallurgical Transactions, Vol. 3, pp. 1807-1816.
- Mackey, P. J., and N. A. Warner, 1973, "Studies in the Vaporization of Mercury in Irrigated Packed Beds," Chemical Engineering Science, Vol. 28, pp. 2141-2154.
- Mamantov, G., J. Braunstein, and C. Mamantov, eds, 1981, Advances in Molten Salt Chemistry, Vol. 4, New York: Plenum Press.
- McCormick, J. L., and E. Baer, 1963, "On the Mechanism of Heat Transfer in Dropwise Condensation," Journal of Colloid Science, Vol. 18, pp. 208.
- Moiseev, G. K., and G. K. Stepanov, 1967, "Surface Wetting of Some Materials By Molten Carbonates of Alkali Metals," Electrochemistry of Molten and Solid Electrolytes, A. N. Baraboshkin, ed., Vol. 5, pp. 101-109, New York: Consultants Bureau.
- Nusselt, W., 1923, Zeitschrift des Vereines Deutscher Ingenieure, Vol. 67, pp. 206-210.
- Onda, K., H. Takeuchi, and Y. Koyama, 1967, "Effect of Packing Materials on the Wetted Surface Area," Kagaku Kogaku, Vol. 31, No. 2, pp. 126-134.
- Onda, K., H. Takeuchi, and Y. Okumoto, 1968, "Mass Transfer Coefficients Between Gas and Liquid Phases in Packed Columns," Journal of Chemical Engineering of Japan, Vol. 1, pp. 56-62.
- Schotte, W., 1960, "Thermal Conductivity of Packed Beds," AIChE Journal, Vol. 6, No. 1, pp. 63-67.
- Standish, 1968, "Heat Transfer in Liquid Metal Irrigated Packed Beds Counter-current to Gases," Transactions of the Metallurgical Society of AIME, Vol. 242, pp. 1733-1740.
- Taecker, R. G., and O. A. Hougen, 1949, "Heat, Mass Transfer of Gas Film in Flow of Gases Through Commercial Tower Packings," Chemical Engineering Progress, Vol. 45, No. 3, pp. 188-193.
- Whitaker, S., "Forced Convection Heat Transfer Correlations for Flow in Pipes, Past Flat Plates, Single Cylinders, Single Spheres, and for Flow in Packed Beds and Tube Bundles," AIChE Journal, Vol. 18, No. 2, pp. 361-371.



Yagi, S., and D. Kunii, 1957, "Studies on Effective Thermal Conductivity in Packed Beds," AICHE Journal, Vol. 3, No. 3, pp. 373-380.

Young, M. L., and J. B. See, 1976, "Effective Thermal Conductivities of Packed Beds of Chromite Ores," Journal of the South African Institute of Mining and Metallurgy, Vol. 77, No. 5, pp. 103-113.

**SELECTED DISTRIBUTION LIST**

Argonne National Laboratory  
9700 S. Cass Ave., Bldg. 362  
Argonne, IL 60439  
A. I. Michaels

Battelle Pacific Northwest  
Laboratory  
P.O. Box 999  
Richland, WA 99352  
L. D. Kannberg

Brookhaven National Laboratory  
Upton, NY 11973  
Al Mezzina

Oak Ridge National Laboratory  
P.O. Box Y  
Building 9204-1  
Oak Ridge, TN 37830  
James Martin

Rockwell International Corp.  
Energy System Group  
8900 De Soto Ave.  
Canoga Park, CA 91304  
Art Kohl

Tom Tracey  
6922 South Adams Way  
Littleton, CO 80122

U.S. Department of Energy  
Forrestal Bldg. (5E-036)  
1000 Independence Ave. S.W.  
Washington, DC 20585  
Kenneth W. Klein

U.S. Department of Energy  
Division of Solar Thermal Technology  
Forrestal Bldg.  
1000 Independence Ave. S.W.  
Washington, DC 20585  
Howard S. Coleman, Director  
Charles Mangold  
Martin S. Scheve  
Tex Wilkins

U.S. Department of Energy  
Office of Energy Storage and  
Distribution  
Forrestal Bldg. (5E-052)  
1000 Independence Ave. S.W.  
Washington, D.C. 20585  
Michael Gurevich  
Eberhart Reimers

DOE/SERI Area Office  
1617 Cole Blvd.  
Golden, CO 80401  
Steve Sargent

<b>Document Control Page</b>	1. SERI Report No. SERI/TR-252-3056	2. NTIS Accession No.	3. Recipient's Accession No.
4. Title and Subtitle Modeling High-Temperature Direct-Contact Heat Exchange in An Irrigated Packed Bed	5. Publication Date September 1987		6.
	7. Author(s) Mark S. Bohn		8. Performing Organization Rept. No.
9. Performing Organization Name and Address Solar Energy Research Institute A Division of Midwest Research Institute 1617 Cole Boulevard Golden, Colorado 80401-3393	10. Project/Task/Work Unit No. 4275.100		11. Contract (C) or Grant (G) No. (C) (G)
	12. Sponsoring Organization Name and Address		13. Type of Report & Period Covered Technical Report
15. Supplementary Notes			14.
16. Abstract (Limit: 200 words) <p>This report presents an analytical model of direct-contact heat exchange (DCHX) in an irrigated packed bed at high temperatures. The specific application is heat exchange between molten salt and air where the molten salt is a sensible heat storage medium and high temperature air is required for an end process. The model defines several heat transfer mechanisms between the three components in the bed--the liquid, the gas, and the packing. It also includes the effect of conduction in the packing. Correlations found in the literature are used to calculate the associated heat transfer coefficients. The model is restricted to liquids that wet the packing material and to gas/liquid flow rates below the loading point. Three dimensionless equations describe the heat balance between the three bed components. The resulting dimensionless parameters reveal that for commercial DCHX systems, radiation heat transfer is unimportant relative to the convective heat transfer, which is consistent with previous experimental results for air/mercury and nitrogen/molten lead systems.<sup>3</sup> The model also predicts volumetric heat transfer coefficients of about 10,000 W/m<sup>3</sup>K, which is consistent with experimental work.</p>			
17. Document Analysis a. Descriptors Direct-Contact Heat Exchangers; Solar Process Heat; Molten Salts; Thermochemical Heat Storage.  b. Identifiers/Open-Ended Terms  c. UC Categories 62a			
18. Availability Statement National Technical Information Service U.S. Department of Commerce 5285 Port Royal Road Springfield, Virginia 22161		19. No. of Pages 41	20. Price A03